JACS
JOURNAL OF THE AMERICAN CHEMICAL SOCIETY
Article
pubs.acs.org/JACS

Study of Nucleation and Growth Mechanism of the Metallic Nanodumbbells

Galyna Krylova,[†] Lisandro J. Giovanetti,[‡] Felix G. Requejo,[‡] Nada M. Dimitrijevic,[†,§] Alesia Prakapenka,[†,∥] and Elena V. Shevchenko*[,†]

[†]Center for Nanoscale Materials, Argonne National Laboratory, Argonne, Illinois 60439, United States

[‡]INIFTA, CONICET and Dto. Física, Facultad de Ciencias Exactas, Universidad Nacional de La Plata, P.O. Box 16, Suc. 4, 1900 La Plata, Buenos Aires, Argentina

[§]Chemical Sciences and Engineering Division, Argonne National Laboratory, Argonne, Illinois 60439, United States

[∥]University of Illinois at Urbana−Champaign, Champaign, Illinois 61820, United States

Supporting Information

ABSTRACT: We propose a general nucleation and growth model that can explain the mechanism of the formation of $CoPt_3$/Au, FePt/Au, and Pt/Au nanodumbbells. Thus, we found that the nucleation event occurs as a result of reduction of Au^+ ions by partially oxidized surface Pt atoms. In cases when Au^{3+} is used as a gold precursor, the surface of seeds should be terminated by ions (e.g., Co^{2+}, Pb^{2+}) that can reduce Au^{3+} to Au^+ ions, which can further participate in the nucleation of gold domain. Further growth of gold domain is a result of reduction of both Au^{3+} and Au^+ by HDA at the surface of gold nuclei. We explain the different ability of $CoPt_3$, Pt, and FePt seeds to serve as a nucleation center for the reduction of gold and further growth of dumbbells. We report that the efficiency and reproducibility of the formation of $CoPt_3$/Au, FePt/Au, and Pt/Au dumbbells can be optimized by the concentration and oxidation states of the surface ions on metallic nanocrystals used as seeds as well as by the type of the gold precursor.

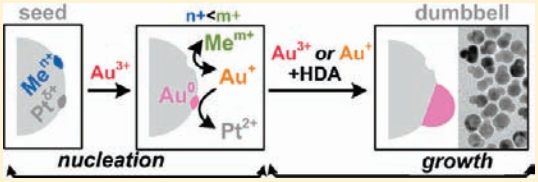

1. INTRODUCTION

Multicomponent nanocrystals (NCs) became an important class of materials due to their abilities to carry multiple functions that can be simultaneously utilized.[1−12] In addition to synergetic properties, multicomponent nanostructures can reveal new collective phenomena originating from the interactions of their building blocks or enhancement of the properties of certain constituents.[1,13−16] Optimization of the composition and electronic structure of nanosized materials is an important direction toward design of better fuel cells,[17] catalysts,[18] MRI,[6,19] and hyperthermia agents,[20] etc. Using a scalable wet chemistry approach, it is possible to combine different materials in the form of individual NCs and synthesize different types of NCs in a form of core−shells,[3,8,13,16] dumbbells,[1,6,18,19,21−30] or other geometries[5,11] and tune the composition of NCs. Metallic multicomponent NCs are of a great interest due to their superior catalytic properties. For example, metallic multicomponent nanocatalysts showed significantly higher activity and stability as compared to single component systems.[17]

Synthesis of multicomponent NCs is typically based on the nucleation of the second component on the seed material.[11,31−33] Despite recent progress in the synthesis of multicomponent NCs, the mechanism of nucleation and growth in such systems is often unclear. Understanding the reaction mechanism is a key step in material design in a controllable way. In our report, using three types of seeds: Pt, FePt, and $CoPt_3$ we analyzed in detail the role of different factors such as concentrations, surface termination, type of gold precursor, etc. in promotion or prevention of the formation of $CoPt_3$/Au, FePt/Au, and Pt/Au dumbbells. Our data provide insight into the mechanism of nucleation and growth of nanodumbbells. In addition to that, we propose the general strategy to synthesize Pt/Au, FePt/Au, and $CoPt_3$/Au nanodumbbells in a controllable way.

2. EXPERIMENTAL SECTION

Chemicals. Platinum acetylacetonate ($Pt(acac)_2$, Acros Organics, 98%); platinum(II) chloride ($PtCl_2$, Aldrich, 98%); chloroplatinic acid hydrate ($H_2PtCl_6 \times 6H_2O$, Aldrich, ≥99.9%); dicobalt octacarbonyl, ($Co_2(CO)_8$, stabilized with 1−5% of hexane, Strem); Iron pentacarbonyl ($Fe(CO)_5$, Aldrich, 99.999%); gold(III) chloride ($AuCl_3$, Aldrich, 99.99%); gold(I) chloride (AuCl, Aldrich, 99.9%); cobalt(II) chloride hexahydrate ($CoCl_2 \times 6\ H_2O$, Aldrich, 98%), cobalt(III) acetylacetonate ($Co(acac)_3$, 99.99%, Aldrich); lead(II) oxide (PbO, Aldrich, 99.99%); copper(I) chloride (CuCl, Aldrich, 99.995+%); iron(II) chloride tetrahydrate ($FeCl_2 \times 4H_2O$ Aldrich, 99.99%); sodium chloride (NaCl Aldrich, 99.99%); silver acetate (CH_3COOAg, Fluka, ≥99%); diphenyl ether (DPE, Aldrich, 99%); 1,2-dichlorobenzene (DCB, anhydrous, Aldrich, 99%); 1-octadecene (ODE, Aldrich, 90%); toluene (Aldrich, 99.5%); chloroform (Aldrich, 99.9%); ethanol (anhydrous, ASC grade, Pharmaco-Aaper); isopropanol (Fisher Scientific, 99.9%); methanol (Riedel-de Haen, 99.9%);

Received: December 7, 2011
Published: February 14, 2012

   dx.doi.org/10.1021/ja211459p | J. Am. Chem. Soc. 2012, 134, 4384−4392

acetone (Fisher Scientific, 99.7%); octylamine (Aldrich, 99%); hexadecylamine (HDA, Aldrich, 90%); oleylamine (Acros, C18-content 80−90%); 1-adamantanecarboxylic acid (ACA, Aldrich, 99%); oleic acid (OA, Aldrich, 90%); trioctylphosphine oxide (TOPO, Aldrich, 99%); tetrakis(decyl)ammonium bromide (TDAB, Aldrich, 99%); didodecyldimethylammonium bromide (DDAB, Fluka, 98%); dodecylethyldimethylammonium bromide (DEDMAB, Aldrich, 98%); 6 M HCl solution (Fisher Scientific); $NaBH_4$ (98.5%, Aldrich); 1,2-dipalmitoyl-*sn*-glycero-3-phosphoethanolamine-*N*-[methoxy-(polyethyleneglycol)-2000] (PEG-PE) dissolved in chloroform (10 mg/mL solution, Avanti Polar Lipids, Inc.); 5,5-dimethyl-1-pyrroline n-oxide (DMPO, 97%, Sigma); H_2O_2 (30%Aldrich) were used as received without any further purification.

Synthesis of 3.0, 8.0, and 11.0 nm $CoPt_3$ NCs. $CoPt_3$ NCs of three different sizes were synthesized according to modified protocol described in ref 34.· Briefly, $Pt(acac)_2$ (0.033 g) and ACA (0.25 g) were dissolved at 55 °C under nitrogen flow in a mixture of HDA (4 g) and DPE (2 mL). Then the solution was heated up to 170 °C (to 200 °C for 3.0 nm $CoPt_3$) and $Co_2(CO)_8$ dissolved in ∼1 mL of DCB was injected. The size of $CoPt_3$ NCs is controlled by the temperature and by the amount of $Co_2(CO)_8$. Thus, 0.106, 0.09, and 0.068 g of $Co_2(CO)_8$ were used to synthesized 3.0, 8.0, and 11.0 nm $CoPt_3$ NCs, respectively. No 1,2-hexadecandiol was used as compared with ref 34. After injection of cobalt carbonyl solution, the reaction mixture was kept at 170 °C (200 °C for 3.0 nm $CoPt_3$) for 1 h. NCs were annealed at ∼246 °C for 15−20 min and then the reaction solution was cooled down to 70 °C and 5 mL of chloroform was injected. After that, the solution was cooled down to the room temperature under ambient conditions.

Synthesis of 2.8 nm Spherical Pt NCs. $PtCl_2$ (0.03 g) and DDAB (0.1 g) were dissolved in 10 mL of toluene by sonication for 30 min. After that OA (0.2 mL) was added and the reaction mixture was sonicated for an additional 5 min and quickly heated to 80 °C. A 40-μL portion of $NaBH_4$ solution in water (0.35 g/mL) was injected into the reaction mixture followed by immediate addition of HDA (0.153 g). The solution was kept at 80 °C for 15 min. The inert atmosphere was not found to be important for synthesis of Pt NCs.

Synthesis of 6.6 nm Cubic Pt NCs. Synthesis was performed according to ref 35 using a modified liquid−liquid biphasic method. Briefly $H_2PtCl_6 \times xH_2O$ (0.084 g) was dissolved in 2.5 mL of deionized (DI) water and 2.5 mL of 1N HCl solution were added. Then phase transfer agent TDAB (0.5 g) was dissolved in 40 mL of toluene. After this, two solutions were mixed and left stirring until the phase transfer was complete (until aqueous solution became transparent and the toluene phase turned orange, indicating the formation of TDAB−Pt complex). Next, a 10-mL portion of toluene solution was taken and bubbled with nitrogen and transferred into a nitrogen glovebox. $NaBH_4$ (0.378 g) was dissolved in 10 mL of DI water and added dropwise to the toluene solution of TDAB−Pt complex. Then the biphasic mixture was sealed and stirred for 3 h before 1 mL of octylamine was added. After that, the solution was left for 16 h. Pt NCs formed in the toluene phase were separated from water solution and washed with alcohols.

Synthesis of 6.8 nm FePt NCs. FePt NCs were synthesized by the modified method reported in ref 36. For this, 0.1 g of $Pt(acac)_2$ was mixed with 7.5 mL of ODE. After evacuating the system at 60 °C for 30 min, the mixture was heated to 120 °C under N_2, resulting in complete dissolution of $Pt(acac)_2$. Subsequently, 0.07 mL of $Fe(CO)_5$ dissolved in 0.9 mL of OA was introduced into the flask by fast injection. After 2−3 min, 1.17 mL of oleylamine was added to the reaction mixture, which was subsequently heated to 200−220 °C and kept at this temperature for 1 h. The color of the reaction mixture gradually turned black, indicating the nucleation of FePt. At this point, the solution was allowed to cool to room temperature. The flask was either opened to air or solution of the FePt NCs was carefully collected with the syringe and quickly transferred into the glovebox in order to minimize the contact of the NCs with moisture or air. Then, a solution of FePt NCs was washed with acetone several times and redissolved in toluene.

Synthesis of $CoPt_3$/Au Dumbbells. Two approaches were used to synthesize $CoPt_3$/Au dumbbells. In a *standard* approach, we used a modified procedure described in ref 37. $CoPt_3$ NCs used as seeds typically contained ∼5−7 wt % of organic molecules (Figure S5 of the Supporting Information, SI). $AuCl_3$ (4 mg), DDAB (28 mg), and HDA (38 mg) were dissolved in 6 mL of toluene by sonication until the clear yellow solution was formed (∼15 min) (note, we used HDA instead of DDA as compared to ref 27). This solution was heated up to 95 °C in three-neck flask. After that ∼50 μL of toluene solution containing 0.57 mg of 8 nm $CoPt_3$ NCs (mass ratio of seeds to gold precursor was ∼1 to 7) was quickly injected into the hot solution of Au precursor. The nucleation and growth of Au was monitored by measuring the absorption spectra during the synthesis. Typically, development of Au surface plasmon band stabilizes after 5−6 h. Thus, reaction solution was left at 95 °C for ∼5−6 h. Then solution was cooled down to room temperature and washed with methanol. In the second approach, a toluene solution of $CoPt_3$ containing 0.57 mg of 8 nm NCs was diluted to 3 mL and heated to 95 °C in a three-neck flask under nitrogen. Then $AuCl_3$ solution in toluene (3 mL) was added dropwise (1 mL/h) via a syringe pump. After that, the solution was kept at 95 °C for two more hours.

The size of Au domain in dumbbells obtained with 8 nm $CoPt_3$ seeds at this ratio was found to be ∼11 nm. In order to control the morphology of the dumbbells, the concentration of $AuCl_3$ was varied in the range from 0.3 to 5 mM that corresponds to the mass ratios of seeds to $AuCl_3$ in the range from 1/1 to 1/16. DDAB (28 mg) and HDA (38 mg) were used as complexing agents and stabilizers. ***Synthesis of Pt/Au and FePt/Au dumbbells:*** We used mostly *standard* procedure described above to synthesize $CoPt_3$/Au dumbbells. Typically concentrations of $AuCl_3$ were 1.88 mM and 2.83 mM in synthesis with Pt and FePt seeds, respectively. These reaction conditions resulted in the formation of Pt/Au and FePt/Au nanodumbbells with slightly larger Au domain.

Postpreparative Procedures. As-synthesized particles were washed to remove the excess of stabilizers and byproducts by precipitation with nonsolvents, such as alcohols (methanol, ethanol, isopropanol). In the case of FePt seeds, acetone was used as a nonsolvent. Subsequent centrifugation was applied to separate aggregates of NCs from their supernatant solutions. Supernatants were discarded and precipitates were redispersed in 2−3 mL of toluene or chloroform and filtered through 0.2 μm PTFE filter. This procedure can be repeated several times if needed.

Study of the Effect of Redox Active Ions on Dumbbell Formation: Co^{2+} Ions. $CoCl_2 \times 6H_2O$ was used as cobalt(II) ions precursor. It is worth mentioning that $CoCl_2 \times 6H_2O$ is not soluble in the nonpolar solvents and in order to transfer Co^{2+} ions into the toluene solution the complexing ability of different organic ligands was tested: OA, ACA, HDA, TOPO, and DDAB. We found that addition of all ligands except HDA resulted in the permanent color change of the initial solution of $CoCl_2$ that we attributed to the formation of the stable complexes with Co^{2+}. In contrast, a mixture of $CoCl_2$ and HDA solution in toluene was reversibly changing color from magenta to blue upon heating to 100 °C and cooling back to room temperature. In order to test the effect of the Co^{2+} concentration on the Au overgrowth on the surface of different seeds, we varied the amount of Co^{2+} in the concentration range from 0.21 to 13.2 mM. Typically, 1 mL of $CoCl_2$ toluene solution containing 30 mg of HDA was mixed with the solution of seeds and injected into the reaction mixture of gold precursor. ***Pb^{2+}ions:*** A 225-mg portion of of PbO was mixed with 5 mL of 1-octadecene and 5 mL of oleic acid. This mixture was heated until 140 °C for 2 h under vacuum in order to complete the formation of lead oleate and to distill the residual water from 1-octadecene. After that solution was cooled to room temperature and ∼130 μL of the solution were mixed with the NCs' seeds and injected into the reaction mixture of gold precursor. ***Cu^{+}ions:*** A 1.3-mg portion of CuCl and 30 mg of HDA were dissolved in 1 mL of toluene by sonication and injected together with seed NCs into the hot reaction mixture of gold precursor.

Study of the Factors Suppressing Au Growth: Co^{3+} Ions. A 4.7-mg portion of $Co(acac)_3$ was dissolved in 1 mL of toluene and

dx.doi.org/10.1021/ja211459p | *J. Am. Chem. Soc.* 2012, 134, 4384−4392

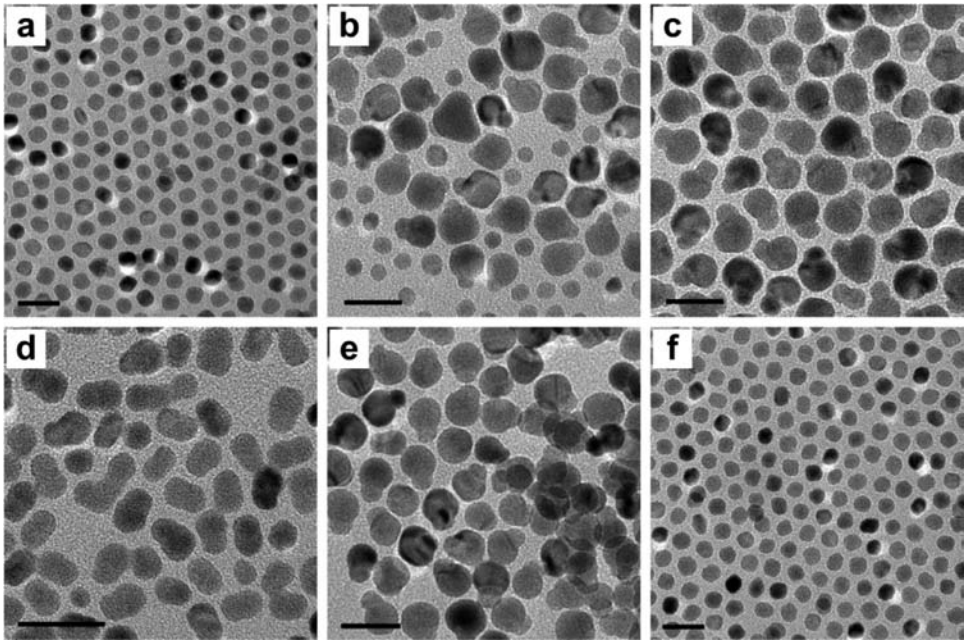

Figure 1. TEM overviews of (a) $CoPt_3$ seeds and $CoPt_3$/Au structures obtained with (b) DDA, (c–f) HDA. Mass ratio of $CoPt_3$ to $AuCl_3$ was 1 to 7 (b,c,e,f) and 1 to 2 (d). Co^{2+} and Cu^{+} ions were introduced into the reaction mixtures in the synthesis of the samples depicted in (e) and (f), respectively. Sample, shown in (e) has been obtained by fast seed injection procedure in the presence of Co^{2+}, while the sample depicted in (c) shows the dumbbells synthesized by slow addition of gold precursor without additional Co^{2+}. Scale bars on TEM images correspond to 20 nm.

injected together with seeds into hot reaction mixture of gold precursor. ***Cl^- ions:*** Two methods of introduction of Cl^- ions were used: (i) 30 mg of HDA were dissolved in 1 mL toluene and NaCl was added during sonication until saturation (~5 mg) and (ii) 30 mg of HDA were dissolved in 1 mL toluene and $CoCl_2 \times 6H_2O$ was added during sonication until saturation (~32 mg). These solutions were further injected into the reaction mixture prior to the seed injection.

Phase Transfer of NCs. NCs were transferred into water according to the protocol described in ref 38. The solutions of NCs were washed by multiple washing steps with alcohols. First washing was performed using the mixture of methanol and ethanol after that washing was performed with ethanol and any other subsequent purification steps were performed with either isopropanol or ethanol/isopropanol mixture. The volume ratio of the NCs solution to the nonsolvent was usually 1 to 10. Final centrifugates were redissolved in 1 mL of chloroform and the PEG-PE dissolved in chloroform (10 mg/mL) was added. The volume of added PEG-PE solution was adjusted to obtain the ratio of PEG-PE molecules and the number of atoms on NCs' surface close to 1 to 5. After addition of phospholipid chloroform was evaporated completely under the nitrogen flow. The solid residue was heated up to 80 °C and 2 mL of hot (80–95 °C) deionized water was added. After cooling the resulting aqueous solution was cleaned from the excess of phospholipid by centrifugation at 20 000 rpm for 2 h. Final aqueous solutions were optically clear and stable for at least 2 weeks.

Dialysis. Aqueous solutions of NCs (1.5 mL) placed into the 0.5–3 mL Slide-A-Lyser dialysis cassette with molecular weight 3500 MWCO were dialyzed versus 300 mL of DI water under stirring. After the dialysis was stopped, the solution was evaporated slowly at 50 °C until its volume became 1.5 mL (equal to the volume of the NCs solution inside the cassette).

Methods. Samples for transmission electron microscopy (TEM) were prepared by dropping and drying of 1–2 μL of toluene solution of NCs on a carbon-coated copper grid (Ted Pella). TEM measurements were performed using a FEI Tecnai F30 microscope operated at 300 kV. X-ray photoelectron spectroscopy (XPS) experiments were performed using the Kratos Axis-165 instrument. Samples were irradiated by a monochromatic Al–K_α X-ray source (15 kV, 10 mA) at an angle of 30 degrees from the sample surface. Photoelectrons were detected by 8 channeltrons of the concentric hemispherical analyzer over an area of 700 × 300 μm, with a spectrometer takeoff angle of zero. The detection was achieved using the constant analyzer energy (CAE) mode. Survey scans were acquired with a pass-energy of 160 eV, 1.0 eV step-size and 100 ms dwell time; while narrow scans were acquired with a pass-energy of 20 eV, 0.1 eV step-size and 200 ms dwell time. All scans were performed with the charge-neutralization system running. Charge-referencing was done with the adventitious carbon peak position of 284.8 eV. The X-ray absorption near edge spectroscopy (XANES) experiments were performed at the XAS-2 beamline of Laboratorio Nacional do Luz Síncrotron, Campinas, São Paulo, Brazil (LNLS). XANES spectra at the Co K-edge (7709 eV) were recorded in air at room temperature in transmission mode with three ion chambers as detectors: one chamber was located before the sample to measure the incident X-ray intensity; the second chamber was arranged after the sample and before the corresponding reference metal foil to measure the intensity after the sample; and the third chamber was after the metal foil. The corresponding spectrum from the metal foil was used to calibrate the absolute energy scale for the corresponding sample spectrum, by positioning the absorption edge at the first inflection point. Monochromator on the beamline was equipped with Si(111) crystals giving the energy resolution of 0.5 eV. The X-ray absorption data reduction was performed using standard procedures:[39] a linear background was fit to the pre-edge region and then subtracted from the entire spectrum, and the jump of the spectrum was normalized to unity with the post edge asymptotic value. The ξ-potential measurements of NCs were performed on ZetaSizer (Mavern Instruments) operating at 633 nm laser wavelength, in the voltage range 0.5–40 V. The ξ-potentials of NCs were measured at 30 V in chloroform. The distance between electrodes was 0.4 cm. The Smoluchowski model was chosen for ξ-potential calculations. The X-ray Diffraction (XRD) was performed at beamline 13-ID-D of the GSECARS sector. The X-ray beam (37 keV energy, corresponding to X-ray wavelength of λ = 0.3344 Å) was focused to a 2 μm diameter spot with a Kirkpatrick-Baez mirror system.

3. RESULTS AND DISCUSSION

In order to synthesize $CoPt_3$/Au, we used the modified procedure previously proposed by T. Pellegrino,[37] and explored

dx.doi.org/10.1021/ja211459p | J. Am. Chem. Soc. 2012, 134, 4384–4392

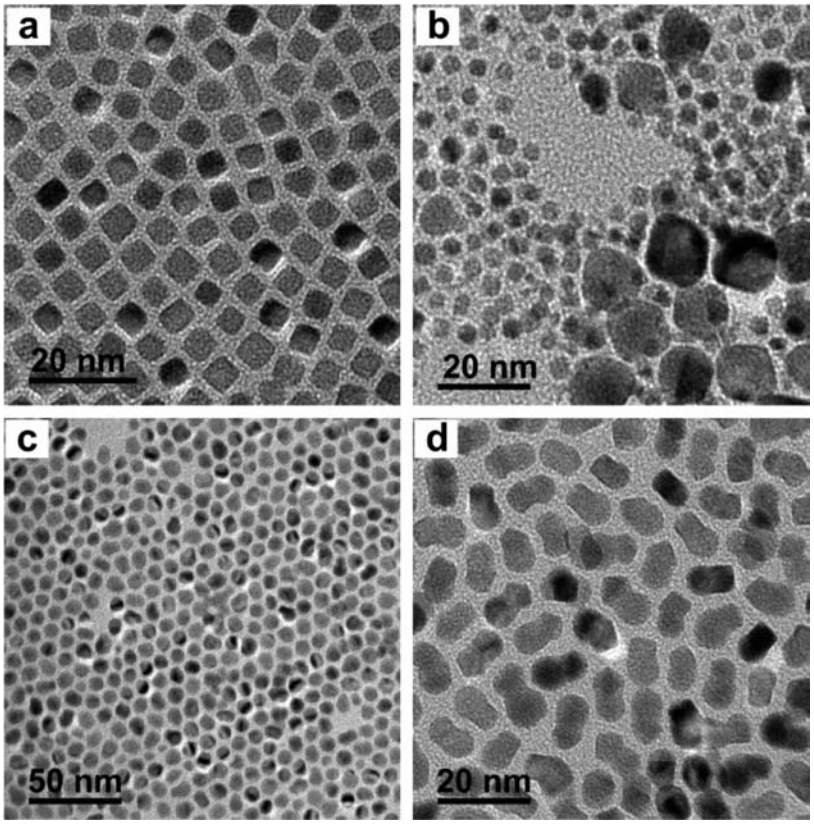

Figure 2. TEM overviews of (a) 6.8 nm Pt seeds and Pt/Au structures obtained with $AuCl_3$ (b), Pt/Au dumbbells synthesized with $AuCl_3$ in the presence of Co^{2+} ions (c), and with AuCl (d). Mass ratio of Pt to gold precursor was 1 to 7. Pt seeds were injected into gold precursor at 95 °C.

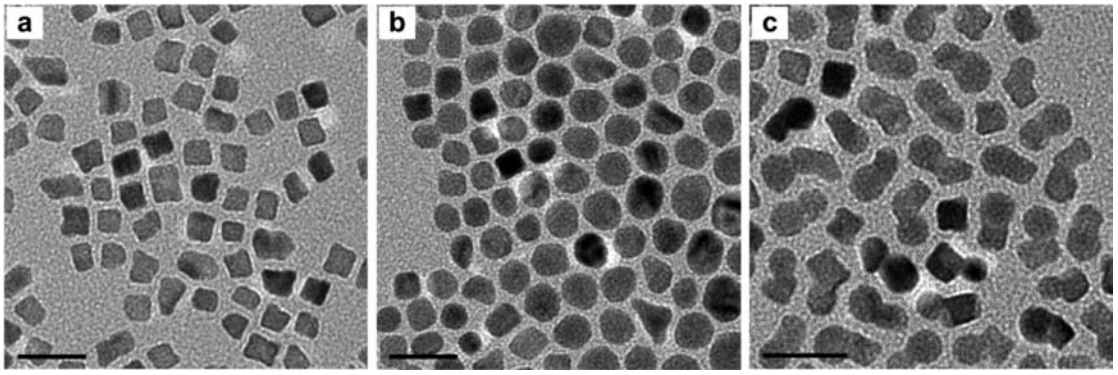

Figure 3. TEM overviews of (a) FePt seeds and FePt/Au structures obtained with FePt* seeds not exposed to air without (b) and with (c) Co^{2+} ions. Mass ratio of FePt to $AuCl_3$ was 1 to 7.

the applicability of this procedure to synthesis of Pt/Au and FePt/Au dumbbells. We found that the replacement of DDA with HDA and higher reaction temperature (95 °C vs 60 °C) improved the yield of $CoPt_3$/Au dumbbells (Figure 1). We applied both (i) fast injection of seeds into reaction mixture containing gold precursor (*standard procedure*) and (ii) dropwise injection of gold precursors into colloidal solution of seeds. In the case of $CoPt_3$ NCs larger than 6.5 nm, both synthetic strategies allowed obtaining monodisperse $CoPt_3$/Au nanodumbbells with high yield, while both methods did not work well for other types of seeds such as 3 nm $CoPt_3$, 6.6 and 2.8 nm Pt, and 6.8 nm FePt. Thus, either no dumbbells were formed or polydisperse and random in shapes gold domains grew only on few Pt seeds (Figures 2 and S1 of the SI). This observation we attributed to the gold nucleation on the defects of the Pt NCs[40] that can have the increased reactivity[41,42] due to their lower atomic coordination numbers.[43,44] In order to explain the difference in the ability of $CoPt_3$, Pt, and FePt seeds to serve as nucleation seeds, we performed a study on the mechanism of nucleation and growth of metallic nanodumbbells.

To date, two basic explanations of the gold nucleation on metallic NCs were proposed.[37,40] Thus, Pellegrino et al.[37] assumed that gold nucleated due to the reduction of Au^{3+} by alkylamine, assuming that the surface of the $CoPt_3$ seeds acts as a catalyst and indeed, it was previously shown that CoPt alloy is more active catalyst in reduction reactions as compared to Pt or FePt.[17] However, Teng et al.[40] suggested that the nucleation of gold at the surface of Pt is a result of the galvanic replacement reaction. The high yield of dumbbells in the case of $CoPt_3$ seeds

dx.doi.org/10.1021/ja211459p | J. Am. Chem. Soc. 2012, 134, 4384−4392

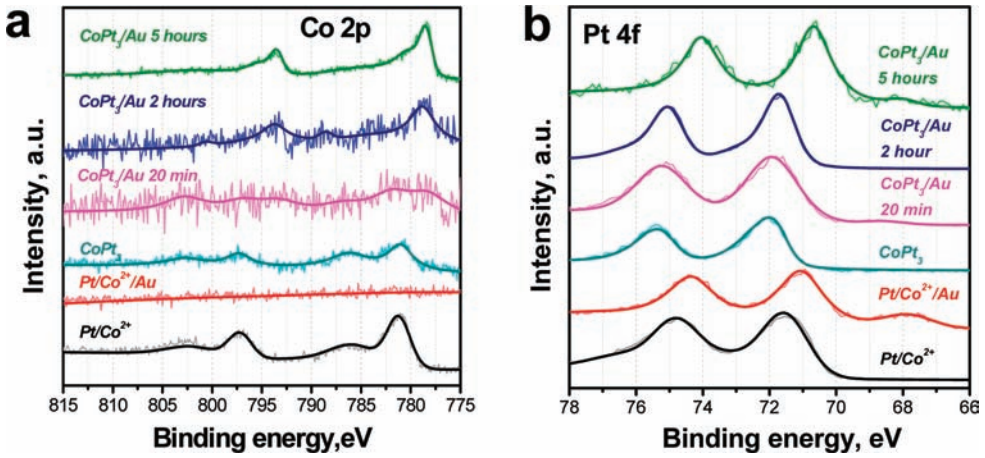

Figure 4. XPS spectra of 8 nm $CoPt_3$, 6.6 nm Pt seeds treated with Co^{2+} ions and $CoPt_3$/Au and Pt/Au dumbbells; (a) Co 2p band and (b) Pt 4f band.

and no formation or low yield of dumbbells obtained when FePt or Pt NCs were used as seeds allowed us to assume that the presence of cobalt on the surface of the seeds, that was confirmed by XPS[45] could promote the gold nucleation. Previously, it was shown that NCs of noble metals tend to accumulate negative charges during their growth and as a result metal cations can be adsorbed on the surface of metallic NCs.[46,47] Thus, we decided to introduce Co^{2+} ions (in a form of HDA-Co^{2+} complex, see the Experimental Section for details) to Pt and FePt seeds before the addition of Au^{3+} precursor (Figures 2 and 3). Indeed, the Co^{2+} ions were adsorbed at the surface of Pt, $CoPt_3$, and FePt NCs stored under nitrogen (further denoted as FePt*) as evidenced by the shift of ζ-potentials toward more positive values upon addition of Co^{2+} (Figure S2 of the SI), whereas FePt NCs exposed to air did not reveal any adsorption of Co^{2+} ions (Figure S2 of the SI). As expected, the introduction of Co^{2+} ions into the reaction mixture resulted in ~100% yield of Pt/Au and FePt*/Au dumbbells, confirming the hypothesis that Co^{2+} ions adsorbed at the surface promoted the formation of dumbbells (Figures 2c and 3c). Blank experiments with and without seeds confirmed no formation of free Au NCs even in the presence of Co^{2+} ions. It is worth mentioning that addition of Co^{2+} ions to $CoPt_3$ seeds allowed the synthesis of monodisperse dumbbells even when fast seed injection procedure was applied (see Experimental Section), which was not the case when Co^{2+} ions were not added (Figure S3 of the SI). The size distribution of gold domains was comparable to that for dumbbells obtained by dropwise method (compare Figure 1c,e).

Pt NCs (6.6 nm) were chosen as a model system to study the effect of concentration of added Co^{2+} ions on the formation of Pt/Au dumbbells. We started with the concentration of Co^{2+} ions equimolar to the concentration of surface cobalt ions on $CoPt_3$ seeds of the same size as Pt seeds. The highest concentration used in the experiments was equimolar with the concentration of added gold precursors. We found that the increase of Co^{2+} concentration resulted in (i) the increase of Pt/Au dumbbells yield and (ii) formation of uniform asymmetric dumbbells with larger gold domains while very low concentrations of Co^{2+} led to (i) the formation of dumbbells with relatively polydisperse gold domains and (ii) decrease of the yields of dumbbells.

The strong adsorption of Co^{2+} ions at the surface of Pt and FePt seeds is confirmed by XPS studies on NCs treated with Co^{2+} ions. Even after three purification steps their surfaces still contain Co^{2+} ions as evidenced by the peak at 781.2 eV (Figures 4a and 6c). However, in Pt/Au dumbbells synthesized

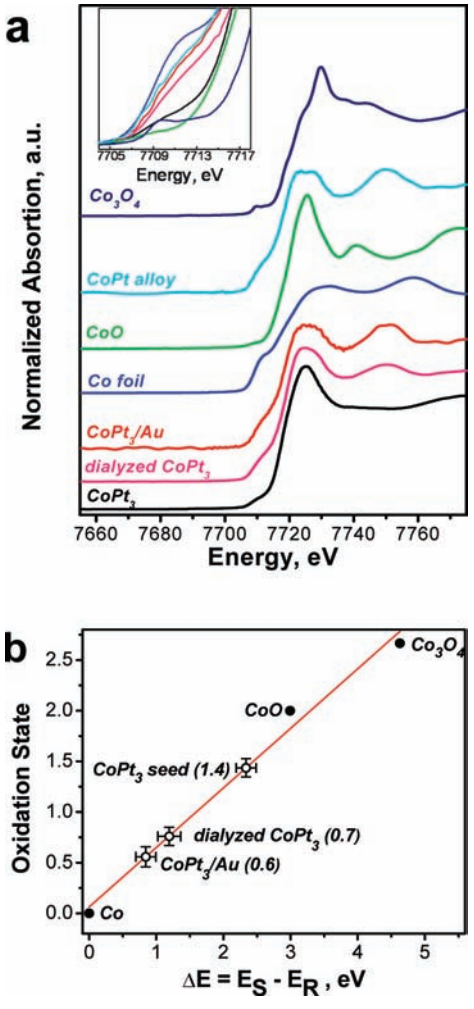

Figure 5. Co K-edge XANES spectra of (a) 8 nm $CoPt_3$ seeds (as prepared and dialyzed) and $CoPt_3$/Au dumbbells; Co foil, CoPt alloy, CoO, and Co_3O_4 standards. The inset magnifies the pre-edge region. (b) Cobalt oxidation states obtained from the calculated energy edge shifts by Capehart's method.[50]

dx.doi.org/10.1021/ja211459p | J. Am. Chem. Soc. 2012, 134, 4384–4392

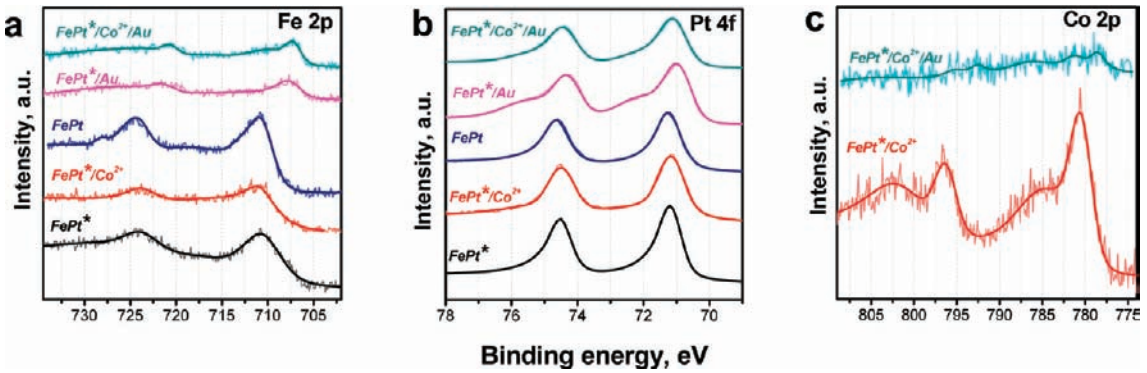

Figure 6. XPS spectra of FePt seeds and FePt/Au dumbbells: (a) Fe 2p band; (b) Pt 4f band; (c) Co 2p band. FePt* corresponds to FePt seeds processed and stored under N_2.

Scheme 1. Depiction of the Mechanism of Nucleation and Growth of X/Au Dumbbells, Where X are NCs of $CoPt_3$, FePt, or Pt and Me^{n+} are Fe^{2+}, Co^{2+}, or Pb^{2+} Cations ($n < m$), Respectively

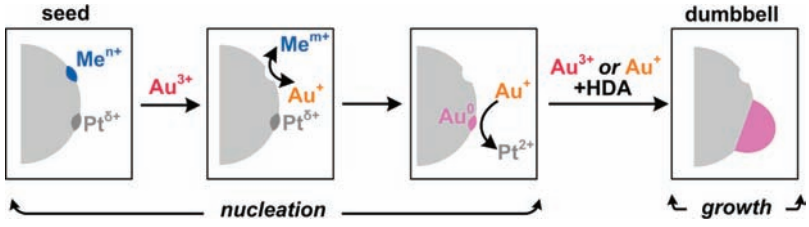

in the presence of Co^{2+} ions, we did not observe any traces of cobalt (Figures 4a and 6c). XPS spectra obtained on the aliquots taken at different reaction times during the synthesis of $CoPt_3$/Au dumbbells also showed that Co^{2+} peak at 781.2 eV gradually disappeared revealing the peak of Co^0 at 778 eV. We assume that the nucleation and growth of the Au domain is accompanied with leaching of surface Co^{2+} ions while Co^0 remains in the core of $CoPt_3$ NCs.

XANES studies on $CoPt_3$ seeds and $CoPt_3$/Au dumbbells also confirm the leaching of Co^{2+} during synthesis of dumbbells (Figure 5). We compared XANES spectrum of $CoPt_3$/Au dumbbells with spectra obtained on dialyzed $CoPt_3$ seeds where surface Co^{2+} ions were leached.[45] Both spectra have shoulders with the intensities similar to the intensity characteristic to Co−Pt alloy. Note that the spectrum of $CoPt_3$ seeds before dialysis is similar in terms of shape and intensity to the spectrum of CoO; however, with more distorted octahedral Co^{2+} sites as it is seen from the stronger resonance in the pre-edge region. We attribute this distortion to the presence of Co atoms coordinated with Pt atoms in chemically disordered alloy and/or surface Co^{2+}.

In order to quantify the average oxidation state, we analyzed the energy edge shift in our samples and different standard cobalt compounds. We found that Co atoms in the initial $CoPt_3$ seeds have higher average oxidation state than in $CoPt_3$/Au dumbbells or in the dialyzed $CoPt_3$ NCs that also confirms the loss of surface Co^{2+} ions during the synthesis of $CoPt_3$/Au dumbbells (Figure 5b).

We also found that gold can nucleate and grow on FePt*, however the yield of FePt*/Au dumbbells was significantly lower as compared to the case of $CoPt_3$ seeds (Figures 3b and 1c, respectively). We assume that FePt* seeds has Fe^{2+} at the surface (Figure 6) that can act similar to Co^{2+}. Addition of Co^{2+} precursor dramatically increased the yield of FePt*/Au dumbbells (Figures 3c and S4 of the SI). According XPS data on FePt*, the nucleation and growth of Au results in the red shift of Fe spectrum revealing metallic Fe^0, which is analogous to the behavior of $CoPt_3$ seeds. Deposition of Au on FePt* seeds exposed to Co^{2+} ions showed that some Fe^{2+} cations still remained on the surface while no detectable signal from Co^0 or Co^{2+} was observed (Figure 6a,c cyan curve). No FePt/Au dumbbells were formed when FePt seeds were exposed to air even in the presence of Co^{2+} that we attribute to (i) the lower stability of Fe(2+) as compared to Co^{2+} and its fast oxidation to Fe(3+)[48] and (ii) no adsorption of Co^{2+} by the surface of oxidized FePt NCs, as indicated by no change in their ζ-potential in the presence of Co^{2+} ions.

Analysis of XPS data obtained for $CoPt_3$-based samples at Pt edge demonstrates that Pt oxidation states also undergo changes during gold deposition (Figure 4b). Thus, in initial $CoPt_3$ seeds, signals corresponding to Pt^0 and $Pt^{\delta+}$ coordinated by ligand[49] were observed at ∼71 and 72.5 eV, respectively (Table S1 of the SI). Growth of gold domain is accompanied by the decrease and increase of the intensity of signals corresponding to $Pt^{\delta+}$ and Pt^0, respectively, following the same trend as in case of Co^{2+} and Co^0. In final $CoPt_3$/Au dumbbells, almost no $Pt^{\delta+}$ (see Figure 4b) can be detected while in the case of FePt*/Au dumbbells (Figure 6b) some amount of $Pt^{\delta+}$ is still present, as evidenced by the small peak at ∼72.3 eV. This difference can be associated with a higher amount of unmodified seeds in the case of FePt as compared with $CoPt_3$ case.

In order to provide further insights into the mechanism of formation of dumbbells we replaced traditional Au^{3+} precursor with Au^+ and observed the formation of dumbbells with high yield even with $CoPt_3$ seeds smaller than 4 nm as well as with Pt and FePt* seeds. Blank experiments with Au^+ precursor and no HDA did not led to the formation of dumbbells indicating that HDA is needed for the growth of Au domains.

Thorough analysis of the experimental data allowed us to make the following conclusions: (i) surface Co^{2+} ions or Co^{2+} ions adsorbed at the surface of metallic seeds are required to

dx.doi.org/10.1021/ja211459p | J. Am. Chem. Soc. 2012, 134, 4384−4392

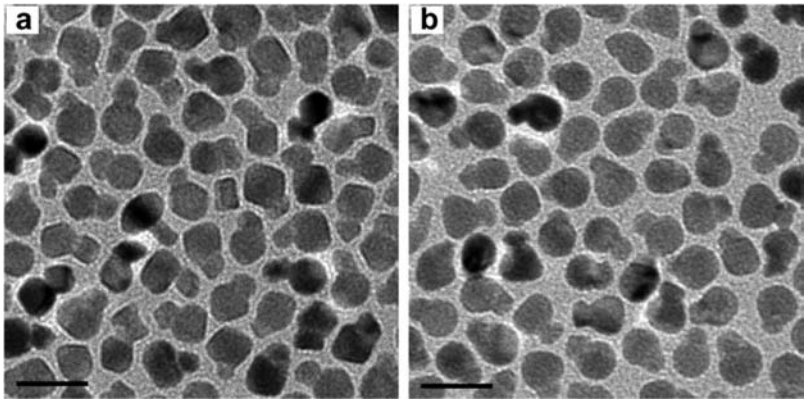

Figure 7. TEM overviews of (a) Pt/Au seeds and FePt/Au dumbbells obtained in the presence of Pb^{2+} ions. Mass ratio of Pt to $AuCl_3$ and FePt to $AuCl_3$ was 1:7.

reduce Au^{3+} to Au^{+}; (ii) partially oxidized platinum atoms, $Pt^{\delta+}$, reduce Au^{+} to Au^{0}, probably, as a result of galvanic replacement, and (iii) both Au^{3+} and Au^{+} can be used as a gold precursor in the presence of HDA during the growth of gold domain (Scheme 1). The role of Fe^{2+} ions is similar to Co^{2+} ions; however, the low stability of Fe^{2+} ions against oxidation makes them less efficient in promoting the formation of dumbbells. Figure S6 of the SI demonstrates the XRD data obtained on $CoPt_3$/Au, Pt/Au and FePt/Au dumbbells.

To get further proof of concept of the proposed reaction mechanism, we analyzed the effect of ions with red/ox properties similar to Co^{2+} and Fe^{2+} on the formation of dumbbells. Thus, Pb^{2+} and Cu^{+} ions were chosen as analogues to Co^{2+} and Fe^{2+} ions, respectively (Figure S7 of the SI). As we expected, addition of Pb(II)oleate to Pt and FePt seeds resulted in the formation of uniform dumbbells with high yield (Figure 7), while the introduction of Cu^{+} ions into the reaction mixture did not promote the synthesis of dumbbells. These observations are in agreement with the proposed mechanism (Scheme 1).

We observed the anisotropic growth of gold under any reaction conditions. Previously, it has been shown that it can be a result of relatively large lattice mismatch between gold and seed materials.[3] In the case of structures with smaller mismatch between Pd and Pt (0.77%), isotropic growth of Pd on Pt seed with core−shell structure formation has been found. It was proven by the Monte Carlo calculations[32] that Au anisotropic growth occurs when the surface energy at the metal−metal interface becomes larger than the surface energy of gold−liquid interface. Control over the mass ratio of seeds to $AuCl_3$ allowed some control over the domain size of Au in dumbbells (Table S1 of the SI). However, we never observed the size of gold domains smaller than the size of seeds. For example, a 1 to 7 mass ratio of 8 nm $CoPt_3$ NCs to $AuCl_3$ precursor (Figure 1c) results in the formation of asymmetric dumbbells with ∼10−12 nm large Au domains indicating ∼71% conversion of gold precursor. Decrease of mass ratio to 1:2 led to the formation of nearly symmetric $CoPt_3$/Au dumbbells (Figure 1d) resulting in ∼78% conversion of gold precursor. Further decrease of $CoPt_3$ to Au mass ratio drastically decreased the yield of dumbbells while increase of the concentration of Au above 1 to 7 mass ratio of 8 nm $CoPt_3$ NCs to $AuCl_3$ did not lead to the increase of the size of Au domains. In most cases, the size of Au domain was below 13 nm. For example, in the case of 11 nm $CoPt_3$ seeds, symmetric dumbbells were obtained at the mass ratio in the range between 1 to 2 and 1 to 14. In the last case, conversion of gold precursor was only ∼16%. The same trend was observed when seeds of other types of NCs were used. Thus, the size of the gold domain did not exceed ∼12 nm when we used 6.6 nm Pt seeds even at high concentrations of $AuCl_3$ (up to 1 to 16 mass ratio of Pt to $AuCl_3$).

These observations allowed us to conclude that the growth of Au domain is limited by some species present in the reaction solution or formed during the synthesis of dumbbells (e.g., Co^{3+} and Cl^{-} ions). We did not observe the suppression of the dumbbell formation when we added excess of Co(III)-acetylacetonate to $CoPt_3$ seeds, while we found that Cl^{-} ions indeed affected the growth of the Au domains in dumbbells. The experiments with addition of saturated solutions of NaCl in toluene led to the formation of symmetric dumbbells under reaction conditions optimized for the formation of asymmetric dumbbells even though the concentration of added Cl^{-} ions was very low because of the very low solubility of NaCl in nonpolar solvents. Also, addition of the saturated solution of $CoCl_2$ ($CoCl_2$ is more soluble in toluene in the presence of HDA than NaCl) to Pt seeds suppressed the formation of Pt/Au dumbbells even though small concentrations of $CoCl_2$ were required to promote the formation of dumbbells when $AuCl_3$ was used as a precursor. Thus, we concluded that growth of Au is affected by Cl^{-} ions that are known to limit the growth of Au.[51−53] Taking into account that we use $AuCl_3$ and AuCl as precursors of gold, Cl^{-} ions are always present in the reaction mixture and can inhibit the gold growth resulting in the focusing of gold domain sizes at high concentration of gold chloride precursors. The absence of free gold and ternary nanoparticles allows us to exclude "tug of war" phenomena[54] in our systems.

4. CONCLUSIONS

We systemically studied the role of the different reaction parameters that can affect the formation of $CoPt_3$/Au, Pt/Au, and FePt/Au dumbbells and explain the different ability of $CoPt_3$, Pt, and FePt seeds to serve as nucleation center for nucleation of gold and the further growth of dumbbells. We propose the mechanism of nucleation and growth. Thus we found that nucleation event occurs as a result of reduction of Au^{+} ions by partially oxidized surface Pt atoms. Further growth of the gold domain is a result of reduction of both Au^{3+} and Au^{+} by HDA at the surface of gold nuclei. The type of the precursor ($AuCl_3$ and AuCl) is found to be critical for the nucleation event. The surface of metallic NCs can be successfully modified

by adsorption of red/ox active cations. In the case when Au^{3+} is used as a gold precursor, the surface of seeds should be terminated by ions (e.g., Co^{2+}, Pb^{2+}) that can reduce Au^{3+} to Au^{+} ions which can further participate in the nucleation of gold domain. The Cl^{-} ions were found to affect the growth of Au domains in dumbbells limiting their sizes to ~12 nm. Understanding the mechanism of the dumbbell formation allowed us to propose a general strategy to synthesize $CoPt_3$/Au, Pt/Au, and FePt/Au dumbbells with precise control over the size distribution and yield of dumbbells.

■ ASSOCIATED CONTENT

Supporting Information

TEM images of 2.8 nm Pt seeds and their Pt/Au dumbbells synthesized by the hot injection of Pt seeds with and without added Co^{2+} cations. The ξ-potentials of Pt and $CoPt_3$ NCs in the toluene solutions as a function of the concentration of added Co^{2+}. TEM images of 3 nm $CoPt_3$ seeds and their $CoPt_3$/Au dumbbells synthesized by dropwise addition of gold precursor to hot $CoPt_3$ seed solution and by hot injection of $CoPt_3$ seeds into the solution of Au precursor in the presence of Co^{2+} cations. TEM images of 6.8 nm cubic FePt* seeds stored under N_2 and their FePt*/Au dumbbells were synthesized by hot injection of FePt seeds into the solution of Au precursor in the presence of Co^{2+} cations. TGA curves of 8 nm $CoPt_3$ seeds before and after purification. XRD patterns of FePt*, $CoPt_3$, and Pt seeds and corresponding dumbbells. Standard electrochemical potentials of transition metal cations compared to the potential of oxygen. Summary table on synthetic conditions of dumbbells. This material is available free of charge via the Internet at http://pubs.acs.org.

■ AUTHOR INFORMATION

Corresponding Author

eshevchenko@anl.gov

Notes

The authors declare no competing financial interest.

■ ACKNOWLEDGMENTS

Work at the Center for Nanoscale Materials was supported by the Office of Science, Office of Basic Energy Sciences, of the U.S. Department of Energy under Contract No. DE-AC02-06CH11357. XANES measurements were partially supported by projects PIP 03079 (CONICET, Argentina), CIAM Argentine-Brazil-Canada collaborative project (CONICET-CNPq-NSERC) PICT 00038 and D04B-XAS 6609/07 (LNLS, Brazil). The XPS results were obtained on the Kratos AXIS-165 operated by the Research Resources Center at the University of Illinois at Chicago. We acknowledge Dr. K.-B. Low for his help with the XPS measurements and data analysis; Dr. A. Demortiere for his help in synthesis of Pt NCs; Dr. V. Prakapenka for his help in XRD measurements, and Dr J. Greely for helpful discussions. A.P. acknowledges the U.S. Department of Energy Summer Undergraduate Laboratory Internship (SULI) program. The use of the Advanced Photon Source was supported by the U.S. Department of Energy, Office of Science, Office of Basic Energy Sciences, under Contract No. DE-AC02-06CH11357. GeoSoilEnviro CARS is supported by the National Science Foundation; Earth Sciences (EAR-0622171) and Department of Energy; Geosciences (DE-FG02-94ER14466).

■ REFERENCES

(1) Li, Y. Q.; Zhang, G.; Nurmikko, A. V.; Sun, S. H. *Nano Lett.* **2005**, *5*, 1689−1692.
(2) Bodnarchuk, M. I.; Kovalenko, M. V.; Groiss, H.; Resel, R.; Reissner, M.; Hesser, G.; Lechner, R. T.; Steiner, W.; Schaffler, F.; Heiss, W. *Small* **2009**, *5*, 2247−2252.
(3) Habas, S. E.; Lee, H.; Radmilovic, V.; Somorjai, G. A.; Yang, P. *Nat. Mater.* **2007**, *6*, 692−697.
(4) Lim, B.; Kobayashi, H.; Yu, T.; Wang, J. G.; Kim, M. J.; Li, Z. Y.; Rycenga, M.; Xia, Y. *J. Am. Chem. Soc.* **2010**, *132*, 2506−2507.
(5) Weili, S.; Hao, Z.; Sahoo, Y.; Ohulchanskyy, T. Y.; Yong, D.; Zhong Lin, W.; Swihart, M.; Prasad, P. N. *Nano Lett.* **2006**, *6*, 875−881.
(6) Gao, J.; Gu, H.; Xu, B. *Acc. Chem. Res.* **2009**, *42*, 1097−1107.
(7) Shevchenko, E. V.; Bodnarchuk, M. I.; Kovalenko, M. V.; Talapin, D. V.; Smith, R. K.; Aloni, S.; Heiss, W.; Alivisatos, A. P. *Adv. Mater.* **2008**, *20*, 4323−4329.
(8) Lee, J.-S.; Bodnarchuk, M. I.; Shevchenko, E. V.; Talapin, D. V. *J. Am. Chem. Soc.* **2010**, *132*, 6382−6391.
(9) Wang, D. S.; Li, Y. D. *J. Am. Chem. Soc.* **2010**, *132*, 6280−6281.
(10) McDaniel, H.; Shim, M. *ACS Nano* **2009**, *3*, 434−440.
(11) Costi, R.; Saunders, A. E.; Banin, U. *Angew. Chem., Int. Ed.* **2010**, *49*, 4878−4897.
(12) Casavola, M.; Falqui, A.; Garcia, M. A.; Garcia-Hernandez, M.; Giannini, C.; Cingolani, R.; Cozzoli, P. D. *Nano Lett.* **2009**, *9*, 366−376.
(13) Dabbousi, B. O.; Rodriguez-Viejo, J.; Mikulec, F. V.; Heine, J. R.; Mattoussi, H.; Ober, R.; Jensen, K. F.; Bawendi, M. G. *J. Phys. Chem. B* **1997**, *101*, 9463−9475.
(14) Mews, A.; Eychmuller, A.; Giersig, M.; Schooss, D.; Weller, H. *J. Phys. Chem.* **1994**, *98*, 934−941.
(15) Guevara, J.; Llois, A. M.; Weissmann, M. *Phys. Rev. Lett.* **1998**, *81*, 5306−5309.
(16) Rodriguez-Gonzalez, B.; Burrows, A.; Watanabe, M.; Kiely, C. J.; Liz-Marzan, L. M. *J. Mater. Chem.* **2005**, *15*, 1755−1759.
(17) Stamenkovic, V. R.; Mun, B. S.; Arenz, M.; Mayrhofer, K. J. J.; Lucas, C. A.; Wang, G. F.; Ross, P. N.; Markovic, N. M. *Nat. Mater.* **2007**, *6*, 241−247.
(18) Jang, Y.; Chung, J.; Kim, S.; Jun, S. W.; Kim, B. H.; Lee, D. W.; Kim, B. M.; Hyeon, T. *Phys. Chem. Chem. Phys.* **2011**, *13*, 2512−2516.
(19) Cheon, J.; Lee, J. H. *Acc. Chem. Res.* **2008**, *41*, 1630−1640.
(20) Pankhurst, Q.; Connolly, J.; Jones, S. K.; Dobson, J. *J.Phys. D: Appl. Phys.* **2003**, *36*, R167−R181.
(21) Wang, C.; Daimon, H.; Sun, S. H. *Nano Lett.* **2009**, *9*, 1493−1496.
(22) Yin, H. F.; Wang, C.; Zhu, H. G.; Overbury, S. H.; Sun, S. H.; Dai, S. *Chem. Commun.* **2008**, 4357−4359.
(23) Wang, C.; Yin, H. F.; Dai, S.; Sun, S. H. *Chem. Mater.* **2010**, *22*, 3277−3282.
(24) Costi, R.; Saunders, A. E.; Elmalem, E.; Salant, A.; Banin, U. *Nano Lett.* **2008**, *8*, 637−641.
(25) Pang, M. L.; Hu, J. Y.; Zeng, H. C. *J. Am. Chem. Soc.* **2010**, *132*, 10771−10785.
(26) Choi, J. S.; Choi, H. J.; Jung, D. C.; Lee, J. H.; Cheon, J. *Chem. Commun.* **2008**, 2197−2199.
(27) Jang, Y.; Kim, S.; Jun, S. W.; Kim, B. H.; Hwang, S.; Song, I. K.; Kim, B. M.; Hyeon, T. *Chem. Commun.* **2011**, *47*, 3601−3603.
(28) Shaviv, E.; Schubert, O.; Alves-Santos, M.; Goldoni, G.; Di Felice, R.; Vallee, F.; Del Fatti, N.; Banin, U.; Sonnichsen, C. *ACS Nano* **2011**, *5*, 4712−4719.
(29) Wu, H. M.; Chen, O.; Zhuang, J. Q.; Lynch, J.; LaMontagne, D.; Nagaoka, Y.; Cao, Y. C. *J. Am. Chem. Soc.* **2011**, *133*, 14327−14337.
(30) Zhang, H. T.; Ding, J.; Chow, G. M.; Dong, Z. L. *Langmuir* **2008**, *24*, 13197−13202.
(31) Cozzoli, P. D.; Pellegrino, T.; Manna, L. *Chem. Soc. Rev.* **2006**, *35*, 1195−1208.
(32) Wang, C.; Tian, W.; Ding, Y.; Ma, Y.-Q.; Wang, Z. L.; Markovic, N. M.; Stamenkovic, V. R.; Daimon, H.; Sun, S. *J. Am. Chem. Soc.* **2010**, *132*, 6524−6529.

(33) Wang, C.; Xu, C. J.; Zeng, H.; Sun, S. H. *Adv. Mater.* **2009**, *21*, 3045−3052.
(34) Shevchenko, E. V.; Talapin, D. V.; Schnablegger, H.; Kornowski, A.; Festin, O.; Svedlindh, P.; Haase, M.; Weller, H. *J. Am. Chem. Soc.* **2003**, *125*, 9090−9101.
(35) Demortiere, A.; Launois, P.; Goubet, N.; Albouy, P. A.; Petit, C. *J. Phys. Chem. B* **2008**, *112*, 14583−14592.
(36) Figuerola, A.; Fiore, A.; Di Corato, R.; Falqui, A.; Giannini, C.; Micotti, E.; Lascialfari, A.; Corti, M.; Cingolani, R.; Pellegrino, T.; Cozzoli, P. D.; Manna, L. *J. Am. Chem. Soc.* **2008**, *130*, 1477−1487.
(37) Pellegrino, T.; Fiore, A.; Carlino, E.; Giannini, C.; Cozzoli, P. D.; Ciccarella, G.; Respaud, M.; Palmirotta, L.; Cingolani, R.; Manna, L. *J. Am. Chem. Soc.* **2006**, *128*, 6690−6698.
(38) Dubertret, B.; Skourides, P.; Norris, D. J.; Noireaux, V.; Brivanlou, A. H.; Libchaber, A. *Science* **2002**, *298*, 1759−1762.
(39) Teo, B. K. In *EXAFS: Basic Principles and Data Analysis (in Inorganic Chemistry Concept ser.)*; Springer: New York, 1986.
(40) Teng, X. W.; Han, W. Q.; Wang, Q.; Li, L.; Frenkel, A. I.; Yang, J. C. *J. Phys. Chem. C* **2008**, *112*, 14696−14701.
(41) *Nanoparticles and Catalysis*; Astruc, D., Ed.; Wiley-VCH Verlag GmbH & Co.: Weinheim, 2008.
(42) Lee, M. T.; Hsueh, C. C.; Freund, M. S.; Ferguson, G. S. *Langmuir* **1998**, *14*, 6419−6423.
(43) Kameoka, S.; Tsai, A. P. *Catal. Lett.* **2008**, *121*, 337−341.
(44) Yatsimirskii, V. K.; Vyaz'mitina, O. M.; Kozlova, T. P. *Theor. Exp. Chem.* **1973**, *7*, 525−529.
(45) Krylova, G.; Dimitrijevic, N. M.; Talapin, D. V.; Guest, J. R.; Borchert, H.; Lobo, A.; Rajh, T.; Shevchenko, E. V. *J. Am. Chem. Soc.* **2010**, *132*, 9102−9110.
(46) Henglein, A. *J. Phys. Chem.* **1993**, *97*, 5457−5471.
(47) Henglein, A. *Chem. Mater.* **1998**, *10*, 444−450.
(48) Vanýsek, P. In *Handbook of Chemistry and Physics*, 90 th ed.; Lide, D. R., Ed.; CRC Press: Boca Raton, FL, 2009.
(49) Dablemont, C.; Lang, P.; Mangeney, C.; Piquemal, J. Y.; Petkov, V.; Herbst, F.; Viau, G. *Langmuir* **2008**, *24*, 5832−5841.
(50) Capehart, T. W.; Herbst, J. F.; Mishra, R. K.; Pinkerton, F. E. *Phys. Rev. B* **1995**, *52*, 7907−7914.
(51) Ha, T. H.; Koo, H. J.; Chung, B. H. *J. Phys. Chem. C* **2007**, *111*, 1123−1130.
(52) Sau, T. K.; Rogach, A. L. *Adv. Mater.* **2010**, *22*, 1781−1804.
(53) Alam, M. J.; Tsuji, M.; Matsunaga, M. *Bull. Chem. Soc. Jpn.* **2010**, *83*, 92−100.
(54) Wang, C.; Wei, Y. J.; Jiang, H. Y.; Sun, S. H. *Nano Lett.* **2009**, *9*, 4544−4547.